Toric honeycomb code

Hyperbolic Floquet code

Checks

$X \bullet\!\!-\!\!\bullet X$
$Y \bullet\!\!-\!\!\bullet Y$
$Z \bullet\!\!-\!\!\bullet Z$

Plaquette stabilisers

HGP code and surface codes of various distances. The shuttling noise is fixed by setting $T*2 = 8$ μs.

r (mod 6)	ISG	Form of $\bar{X}_i$	$\bar{X}_i$ in $\mathcal{T}_c^*$	Form of $\bar{Z}_i$	$\bar{Z}_i$ in $\mathcal{T}_c^*$
0	R	$\mathcal{V}_0^X(P(\bar{X}_i))$	cocycle in $\mathcal{T}_R^*$	$\mathcal{V}_0^Z(P(\bar{Z}_i))$	cycle in $\mathcal{T}_R^*$
1	G	$\mathcal{V}_1^X(P(\bar{X}_i))$	cycle in $\mathcal{T}_G^*$	$\mathcal{V}_1^Z(P(\bar{Z}_i))$	cocycle in $\mathcal{T}_G^*$
2	B	$\mathcal{V}_2^X(P(\bar{X}_i))$	cocycle in $\mathcal{T}_B^*$	$\mathcal{V}_2^Z(P(\bar{Z}_i))$	cycle in $\mathcal{T}_B^*$
3	R	$\mathcal{V}_3^X(P(\bar{X}_i))$	cycle in $\mathcal{T}_R^*$	$\mathcal{V}_3^Z(P(\bar{Z}_i))$	cocycle in $\mathcal{T}_R^*$
4	G	$\mathcal{V}_4^X(P(\bar{X}_i))$	cocycle in $\mathcal{T}_G^*$	$\mathcal{V}_4^Z(P(\bar{Z}_i))$	cycle in $\mathcal{T}_G^*$
5	B	$\mathcal{V}_5^X(P(\bar{X}_i))$	cycle in $\mathcal{T}_B^*$	$\mathcal{V}_5^Z(P(\bar{Z}_i))$	cocycle in $\mathcal{T}_B^*$

Instructions: (1) entangle all ancilla qubits with their South-West data qubit (2) shuttle by $d-1$ increments forwards (3) entangle all ancilla qubits with their North-East data qubit; measure and reinitialize X ancilla qubits (4) shuttle by one increment forwards (5) entangle all ancilla qubits with their South-East data qubit (6) shuttle by $d+1$ increments backwards (7) entangle all ancilla qubits with their North-West data qubit; measure and reinitialize Z ancilla qubits (8) shuttle by one increment forwards (9) repeat

APPENDIX C: GOOD MATRIX FOR HGP CODE

In Secs. IV A and IV C, we simulated the performance of a HGP constructed from the product of a [8,1,8] repetition code and a [17,3,8] classical code generated randomly. Its parity-check matrix H_8 is

$$H_8 = \begin{pmatrix}
0 & 1 & 0 & 0 & 0 & 0 & 0 & 0 & 0 & 0 & 0 & 1 & 0 & 1 & 0 & 0 & 0 \\
1 & 0 & 0 & 0 & 1 & 0 & 0 & 1 & 0 & 0 & 0 & 0 & 1 & 0 & 1 & 0 & 0 \\
1 & 0 & 0 & 0 & 0 & 1 & 1 & 0 & 0 & 0 & 0 & 0 & 0 & 0 & 0 & 0 & 0 \\
0 & 0 & 1 & 0 & 0 & 0 & 0 & 0 & 0 & 0 & 0 & 0 & 0 & 0 & 1 & 0 & 0 \\
0 & 0 & 0 & 0 & 0 & 0 & 0 & 0 & 1 & 0 & 0 & 0 & 0 & 1 & 0 & 0 & 0 \\
0 & 0 & 0 & 0 & 0 & 0 & 0 & 1 & 0 & 0 & 0 & 0 & 0 & 0 & 0 & 0 & 0 \\
0 & 0 & 0 & 0 & 1 & 0 & 0 & 0 & 0 & 0 & 0 & 1 & 0 & 0 & 0 & 0 & 0 \\
0 & 0 & 0 & 0 & 0 & 1 & 0 & 0 & 0 & 1 & 0 & 0 & 0 & 0 & 0 & 0 & 0 \\
0 & 0 & 0 & 0 & 0 & 1 & 0 & 0 & 0 & 0 & 0 & 0 & 0 & 0 & 0 & 1 & 0 \\
0 & 0 & 0 & 0 & 1 & 0 & 0 & 0 & 0 & 0 & 0 & 0 & 1 & 0 & 0 & 0 & 1 \\
0 & 0 & 0 & 0 & 0 & 0 & 0 & 0 & 0 & 0 & 1 & 0 & 0 & 0 & 0 & 0 & 0 \\
0 & 1 & 0 & 1 & 1 & 0 & 0 & 0 & 0 & 0 & 0 & 0 & 0 & 0 & 0 & 0 & 0 \\
1 & 1 & 0 & 0 & 0 & 0 & 0 & 0 & 0 & 0 & 0 & 0 & 0 & 0 & 0 & 0 & 0 \\
0 & 0 & 0 & 0 & 0 & 0 & 0 & 0 & 1 & 0 & 0 & 0 & 1 & 0 & 0 & 1 & 1
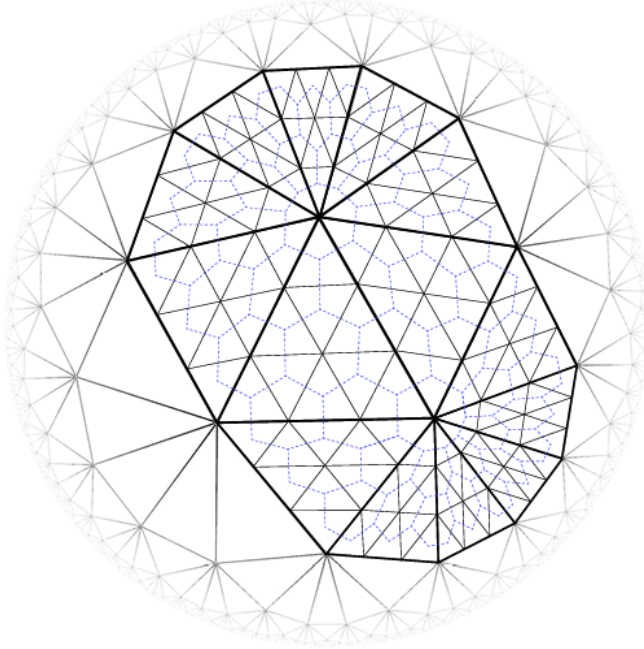\end{pmatrix}.$$

FIG. 4. Obtaining a semi-hyperbolic color-code tiling by fine graining a 3^8 tiling and then taking its dual. We fine grain by tiling each face of the 3^8 tiling with a triangular lattice, such that each side of each face in the 3^8 tiling becomes subdivided into l edges (shown for a subset of the faces here, with $l = 3$). We take the dual of this lattice (blue dashed lines) to obtain a semi-hyperbolic color-code tiling of hexagons and octagons.

padding_error $= 2\,lc\times 4dldd\,(vT*2)2$ Ignoring nonadiabatic effects for now, Eq. 4 of [18] shows that the probability of a dephasing error $\delta\varphi 2/2$ for one shuttle follows: $\delta\varphi 2/$
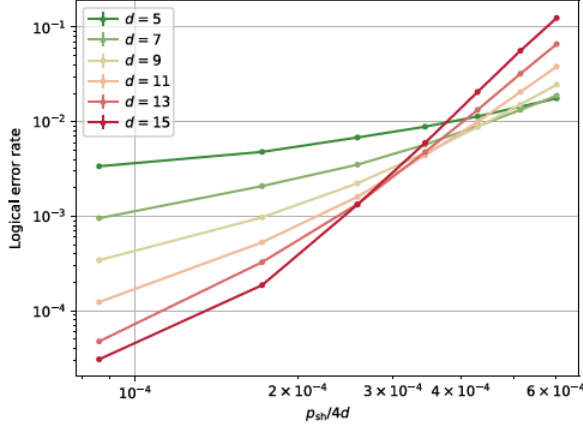
FIG. 8. Logical error rate of a wide surface code against $p_{sh}/4d$, i.e., the probability that one shuttling increment introduces a dephasing error, plotted for several code distances d. The gate, measurement, and initialization noise p is set to 0.1%.

variable_pidle $= 1 - e^{-Tgate/T2} = 5 \times 10^{-5}$. When using this value, one would obtain the same qualitative performance as for the variable_pidle $= 0$ case. Furthermore, here we set a single parameter variable_pidle quantifying the idling error. It would be more comprehensive to distinguish different pidle's depending on the operation that is being waited for. Specifically, as two-qubit gates.

|	$\frac{n+n_{anc}}{k}$	d	Shuttling noise scaling	Idling noise scaling	A	B	C
SC3	25	3	$O(\sqrt{n})$	$O(1)$	2×10^{-4}	1×10^{-4}	3×10^{-4}
GB	9	8	$O(n)$	$O(1)$	7.10^{-3}	5×10^{-5}	7.10^{-3}
HGP4	26	4	$O(\sqrt{n})$	$O(\sqrt{n})$	4×10^{-5}	1.10^{-3}	1.10^{-3}
SC7	169	7	$O(\sqrt{n})$	$O(1)$	1×10^{-5}	3×10^{-6}	1×10^{-5}
HGP8	155	8	$O(\sqrt{n})$	$O(\sqrt{n})$	8×10^{-6}	1×10^{-5}	2×10^{-5}

SURFACE CODES STABILIZER CIRCUIT GATE ORDERING Here we delve into the details of finding an optimal gate ordering for surface-code error correction on the $2 \times N$ architecture. Indeed, the usual pattern that is used for the regular rotated surface code with N-andZ-shaped orderings [68] leads to unnecessarily long shuttles. To see this, assume that the shuttling direction is vertical—two consecutive data qubits within the same column (respectively, row) of the surface code are thus separated by 1 (respectively, d) shuttling increment(s).
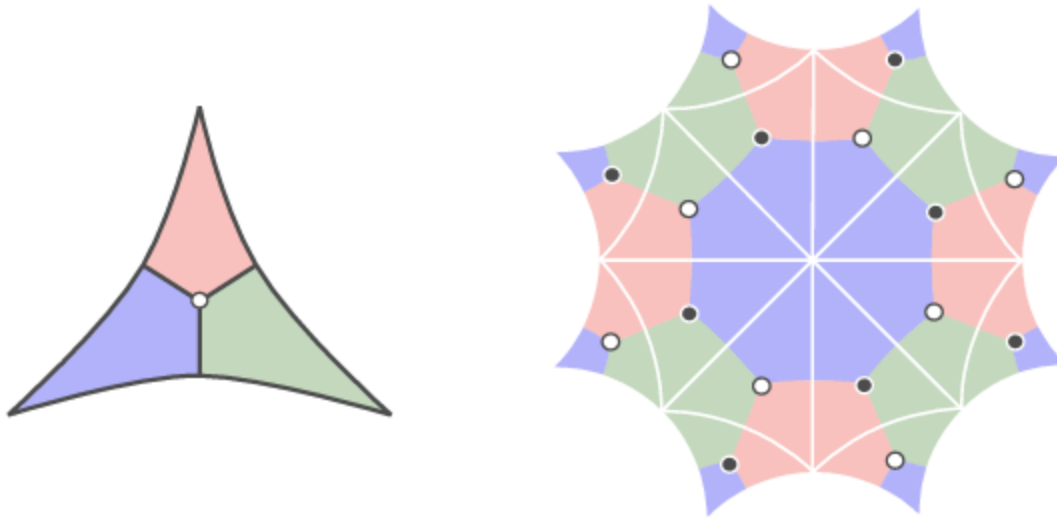
where here $\chi := |V|-|E|+|F|$ is the Euler characteristic of the tiling. We refer the reader to Ref. [37] for further background on homology theory relevant to quantum codes derived from tilings. If T is further a uniform r.g.b color-code tiling we have that nimH 1.2−|V|+|E|−|F| =|V| 1 2 − 1 r − 1 g − 1 b +2.

Union between Quantum channels and blackholes, space materials, space research: Carter–Penrose diagram for the spacetime of a collapsing spherical star that forms a black hole. The part of the spacetime that depicts the triangle with the singularity at the upper side and the event horizon as another side, is invisible from the future null infinity J+. It Describes The black hole interior region. boundary of B in M,H+ = ˙ J−(J+)∩M,iscalledtheeventhorizon. In Other Words, a black hole in asymptotically flat spacetime is defined as region such that no causal signal (i.e.a signal propagating travelocity not greater than that of light) from it can reach future null infinity J+ (see Figure 10.8). The region outside the black hole is called the domain of outer communications.Observer this domain can send causal signals to H+ and receive such signals from J−. Obviously, not just one but several black holes may exist in a bounded region of spacetime; new black holes may be created, andthose already existing may interact and merge. In such cases, ˙ J−(J +) is the union of the boundaries of all black holes. Ifan asymptotically flat space contains no horizon, then all events taking place in this space can be recorded, after an appropriate time, by distant observer.

 Neutron-star–neutron-star (NS–NS) coalescence. The best estimation for the rate density gives: 5×10^{-6} yr−1 Mpc−3. Uncertainty is a factor of the order of 0.01–10; Neutron-star–black-hole (NS–BH)coalescence. The rate density is about 3%of the NS NSrate density; Black-hole–black-hole (BH–BH)coalescence. The rate density is about 0.4%of the NS NSrate density. NS–NS andNS–BHcoalescence events might be responsible for short gamma-ray bursts (see Section 10.3.8). These Events are also of high interest since they in principle can give us information concerning properties of the matter at nuclear densities.
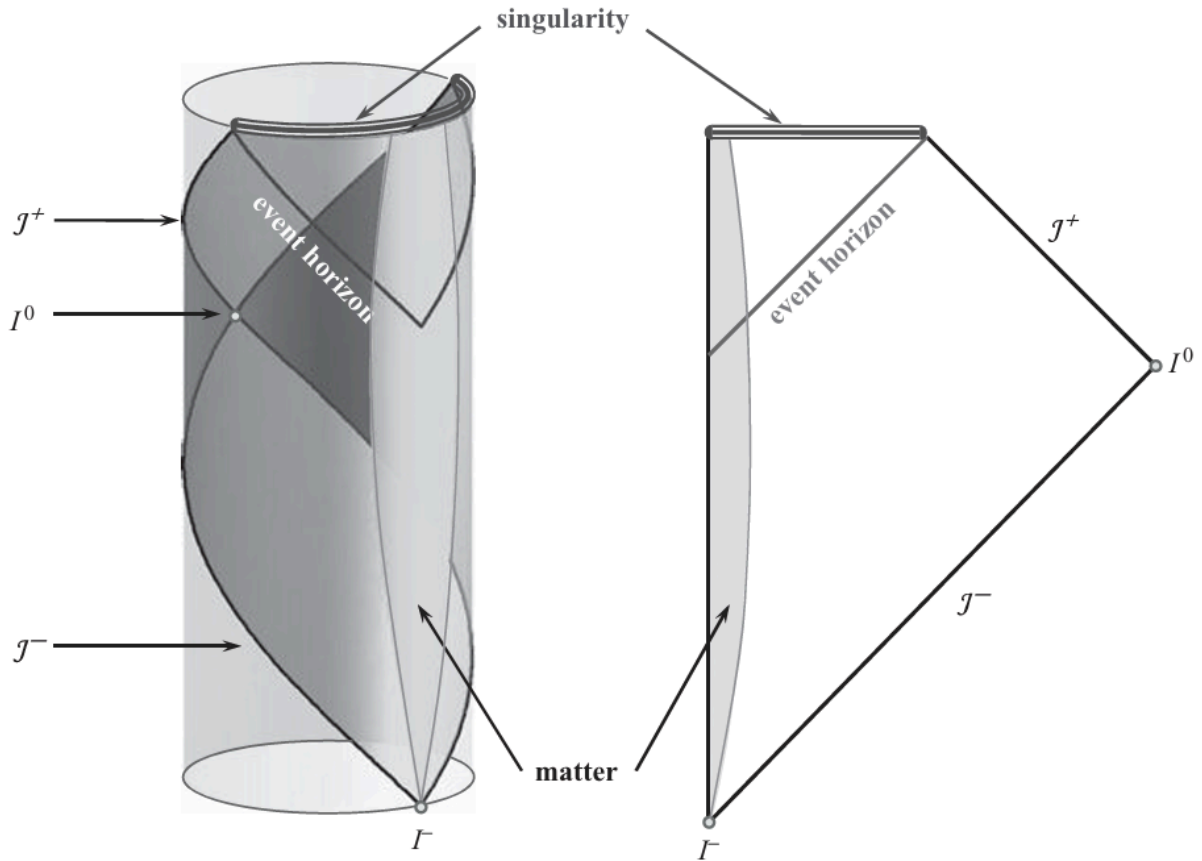
The topology of black holes Black Holes: General Definition and Properties 357 Before discussing the geometry of the event horizon,

Topology: Let t be a one-parameter family of 3D space-like Cauchy surfaces. Such surfaces extend to infinity and cross the horizon.We assume that a surface at given parameter t0 is in the future with respect to surface with the smaller value of the time parameter t < t0.We denote By a two-dimensional space-like surface of intersection of t and the event horizon. One can consider Bt as a horizon surface at the 'given moment of time t'. When one speaks about the topology of black hole one has in mind the topology of these 2D sections Bt. In the general case, there may exist several black holes, so that Bt has several disconnected components. For Simplicity, we assume that only one black hole is present. The following theorem was proved byGannon (1976): The horizon of the blackhole must be either spherical or toroidal, provided the dominant energy condition is satisfied and the horizon smooth to the future of some slice. The latter condition entails in particular that no new generators entering the future that slice. If The topology of the horizon is toroidal it can occur only during a short enough time. This follows from the following result(Friedman et al. 1993): Topological censorship theorem. If an asymptotically flat, globally hyperbolic spacetime satisfies the averaged null-energy condition, then every causal curve from J− to J+ can be continuously deformed to a causal line γ0 totally located in the blackhole exterior the region where the gravitational field is weak.
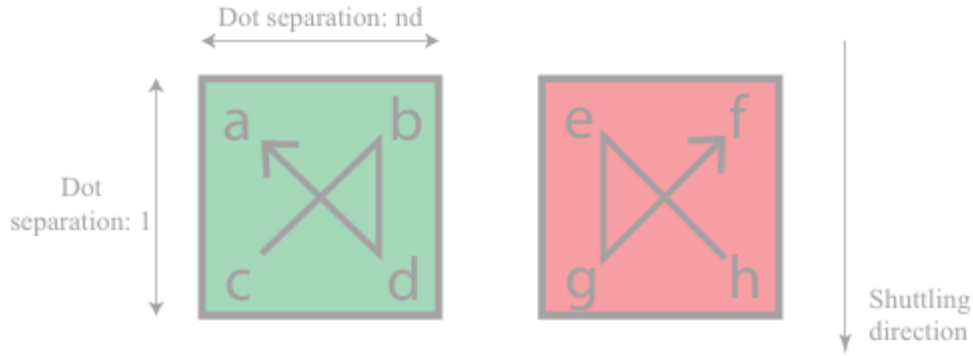
FIG. 13. Notations for conditions (A1)–(A3).

Circ:

FIG. 9. A modular architecture for a semi-hyperbolic Floquet code. Each module has the connectivity of a planar Euclidean chip, and arbitrary connectivity is permitted between modules. In this example, each module is the result of fine graining the neighborhood of one vertex of the seed tiling T used to construct an $l = 3$ semi-hyperbolic Floquet code F(T3). Each long-range connection corresponds to a two-qubit measurement on qubits in two different modules. These inter-module connections may in general be long-range in order to facilitate the necessary connectivity of the semi-hyperbolic Floquet code.
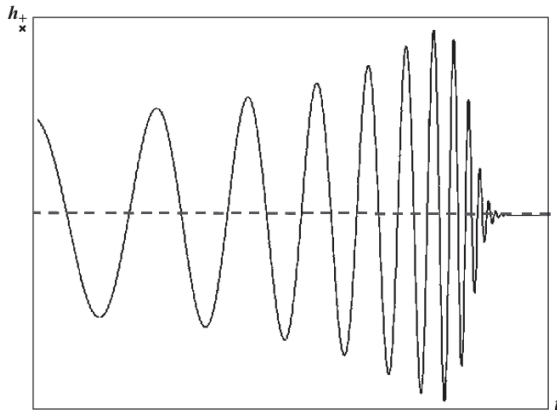
Gravitational-wave detectors Gravitational waves that reach the Earth induce relative motion between separated 'free' masses. To trace these tiny changes of distances it is convenient to use laser interferometers. Thereexist several operational ground-based gravitational-wave detectors. The most sensitive is LIGO–the Laser Interferometer Gravitational WaveObservatory. LIGO has 3 detectors: one in Livingston (Luisiana) and the other two at Hanford (Richmond, Washington). Initial operation of the LIGO detectors began in 2001. Each detector consists of two storage arms, which are vacuum tubes of1m diameter and4k length at the right angle to each other. At Hanford the detector besides the main 4 km interferometer also contains a half-length interferometer using the same vacuum tubes. In November 2005 the sensitivity of the LIGO detectors reached the projected value of 10^{-21} over 100 Hz frequency bandwidth. There are other working ground-based detectors. GEO 600 is the German–British Laser interferometer located near Hannover. It has two arms of length 600 m each. It is working in the frequency range 50Hz–1.5kHz. Its sensitivity is $10^{-20} - 10^{-21}$. The GEO600 detector reached the designed sensitivity in 2006.VIRGO is a gravitational-wave detector at Cascina inItaly. It has two arms

of300 m each. It commenced operations in 2007. TAMA300 is a gravitational-wave detector constructed in Japan. It has two arms of300 m each. In November 2005, LIGO andGEO 600 began a joint science run. In 2007 Virgo joined this collaboration.At the present time there exist a few months of 3-detector data and3 years of 2-detector data. These detectors are effective in the frequency bandwidth required for observation of the gravitational waves from NS–NS, BH–NS, and stellar mass BH–BH binaries. It is Planned To upgrade LIGO. The advancedLIGO,which should be fully operational in 2016,will have sensitivity exceeding the initial LIGOby more than a factor of10. Iti Expected that this new instrument will detect gravitational waves from compact relativistic sources as often as 1 peraday.The jointwork of several existing and newly constructed detectors will give detailed information on the strength and the form of the wave front, as well as a position of the source of the gravitational waves in the sky. The study of the gravitational waves generated by supermassive black holes requires operation in the low-frequency window. The laser Interferometer Space Antenna(LISA)is the most developed project. LISA is plannedasaspace-based laserinterferometer with three test massesforminganequilateral triangle. The frequency window ofLISA is $10^{-4} - 10^{-1}$ Hz. It would be able to see such events as massive (10^6 M) black hole mergers in distant galaxies at $z = 1$, formation of the earliest black holes with 10^4 M at $z = 15$, and stellar-mass black holes captured by the massive black holes. 6As it is adopted in astronomy we give distance in parsecs. 1 pc≈ 3×10^{13} km=3×10^{18} cm; 1 Mpc= 10^6 pc, and1Gpc= 10^9 pc. The cosmological redshift at the distance 6.5Gpc is z ~ 1. The presented estimation of the frequency for the binary system of supermassive black holes takes into account this redshift effect.
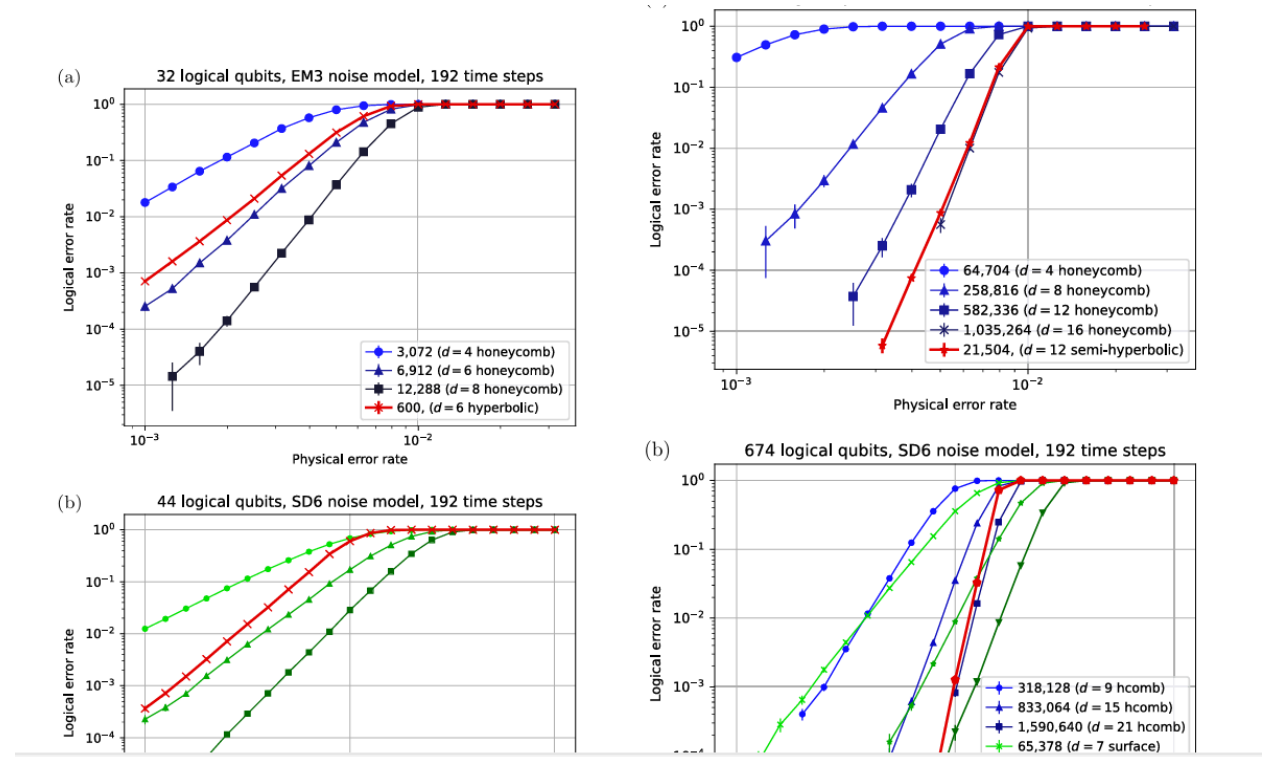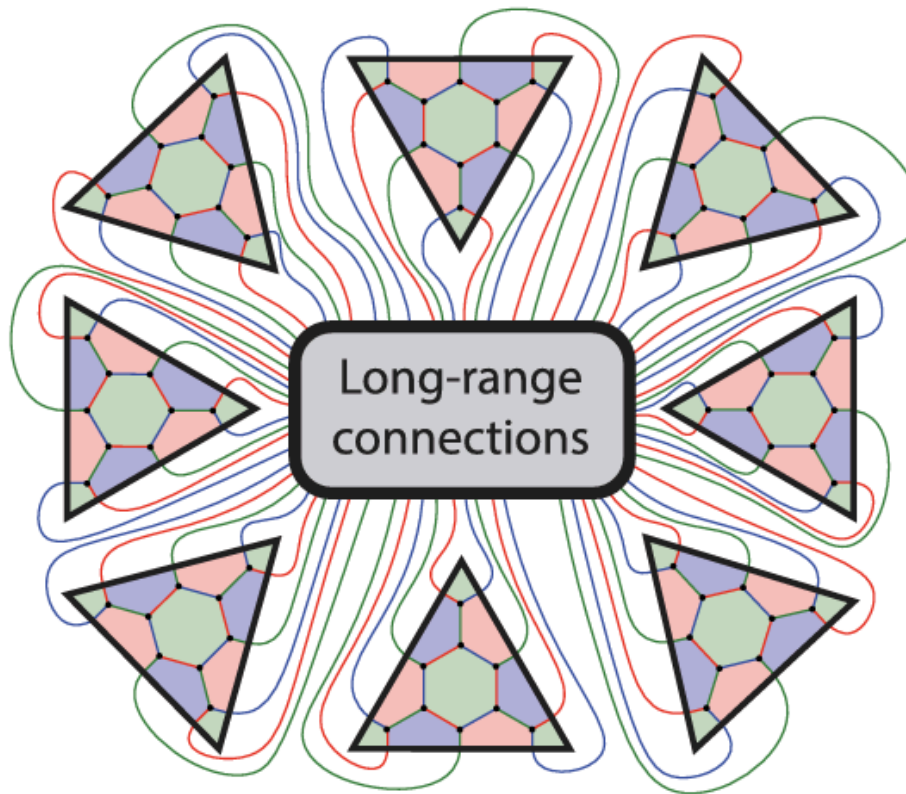
The topological censorship theorem states that general relativity does not allow an observer to probe the topology of spacetime: any topological structure collapses too quickly to allow even the light to traverse it. More precisely, in a globally hyperbolic,asymptotically flat spacetime satisfying the null-energy condition, every causal curve from past null infinity to future null infinity is fixed-endpoint homotopic to a curve in a topologically trivial neighborhood of infinity. If the toroidal topology of the horizon exists for long enough time, acausal line from J− to J+ can pass through the inner region of the torus. Such a curve cannot be deformed smoothly γ0. This is in contradiction with the topological censorship theorem. The described result is a generalization of the famous Hawking theorem (Hawking 1972a, 1972b): Cross-sections of the event horizon 4D asymptotically flat stationary blackhole spacetime obeying the dominant energy condition are topologically two-spheres. It Should be emphasized that in the time-dependent case, 2d Sections Bt depend on the choice of the foliation t.

$r \pmod 6$	$\mathcal{V}_r^X$	$\mathcal{V}_r^Z$
0	Y on red edges	X on green edges
1	Y on blue edges	Z on green edges
2	X on blue edges	Z on red edges
3	X on green edges	Y on red edges
4	Z on green edges	Y on blue edges
5	Z on red edges	X on blue edges

Geometrical properties of the event horizon The following theorem proved byPenrose (1968) describe the geometry of an event horizon: The event horizon is formed by null geodesics (generators) that have no end points in the future. for definitions of this and other energy conditions used in this section. 358 Black Holes and All That Jazz Thus, at the regular points the horizon is a null surface. Ifwemonitoragenerator of the horizon to the future it never leaves the horizon and never intersects another generator. Ifwe monitor a generator of the horizon to the past, two alternatives are possible. To put it simpler, if the asymptotically flat spacetime does not have a naked singularity the Hawkingareatheorem guarantees that the surface area of any black hole either remains the same or monotonically grows provided the matter and fields respect the null-energy condition.
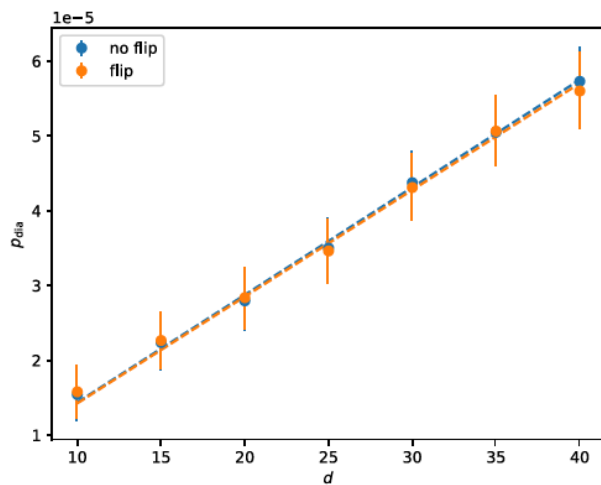
Fractal Quantum Channel and Event Horizon Dynamics

The geometry of the event horizon, as defined by Penrose's theorem, shows that it consists of null geodesics (generators) with no endpoints in the future. These null surfaces ensure that generators neither leave the horizon nor intersect others as they evolve into the future. In asymptotically flat spacetimes without naked singularities, the **Hawking area theorem** dictates that the surface area of a black hole remains constant or grows monotonically, provided the null energy condition holds.

Now, introducing a **fractal quantum channel** into this context, such as the one depicted in the image, provides a new perspective on **acoustic or auditory gravity at a quantum level of frequencies**. The fractal geometry suggests the existence of **extra-dimensional spaces** that arise from quantum wave interactions and frequencies. These dimensions host unique physical phenomena, unexplored by conventional physics, resembling a **wormhole tail** with **intermittent blue lights**.

This "tail" operates as a **quantum frequency pathway**, connecting disparate dimensions and offering insights into:

- **Quantum wave interactions**: How waves at different frequencies produce higher-dimensional phenomena.
- **Acoustic gravity fields**: A novel interpretation of gravitational interactions mediated by sound-like frequencies or wave structures.
- **Special universal events**: These fractal channels could be pathways for extraordinary quantum events, shaping dynamics unseen in the classical universe.

This model integrates Penrose's classical geometric properties with a quantum perspective, revealing a multi-dimensional universe where **blue quantum channels** act as conduits for complex frequency and wave phenomena.

$$H4 = \left(\left| \left\lfloor 1\,0\,0\,1\,1\,0\,1\,0\,0\,1\,0\,1\,0\,1\,0\,1\,1\,0\,0\,1\,0\,1\,0\,1\,0\,1\,1\,0 \right\rangle \right| \right)$$
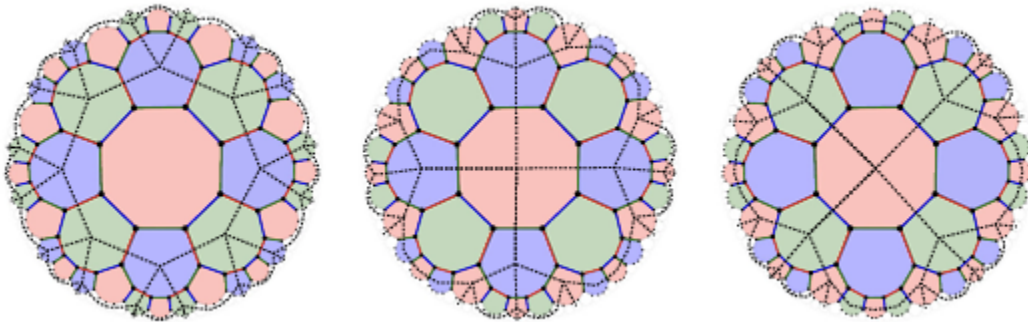
Theembedded2DhomologicalcodeC(T∗ c)associated withtheFloquet code after measuring check soft colors is defined forT∗ c by associating qubits with the edges, Z checks with the faces and X checks with the vertices. An effective ˆXoperatorona Effective Qubit inT∗ c cor responds to a physical Pci operator on theFloquet code data qubits and similarly an effective ˆZ operator corresponds to physical⁻c⊗P⁻c operator,wherehere ⁻c∈ {R,G,B}\{c}.Asanexampleofthismapping,notice that aredX⊗8 plaquette stabilizer inFig.5corresponds toa ˆZ⊗plaquette operator inC(T∗ R)entoan ˆX⊗4 site operatorinC(T∗ G)orC(T∗ B).
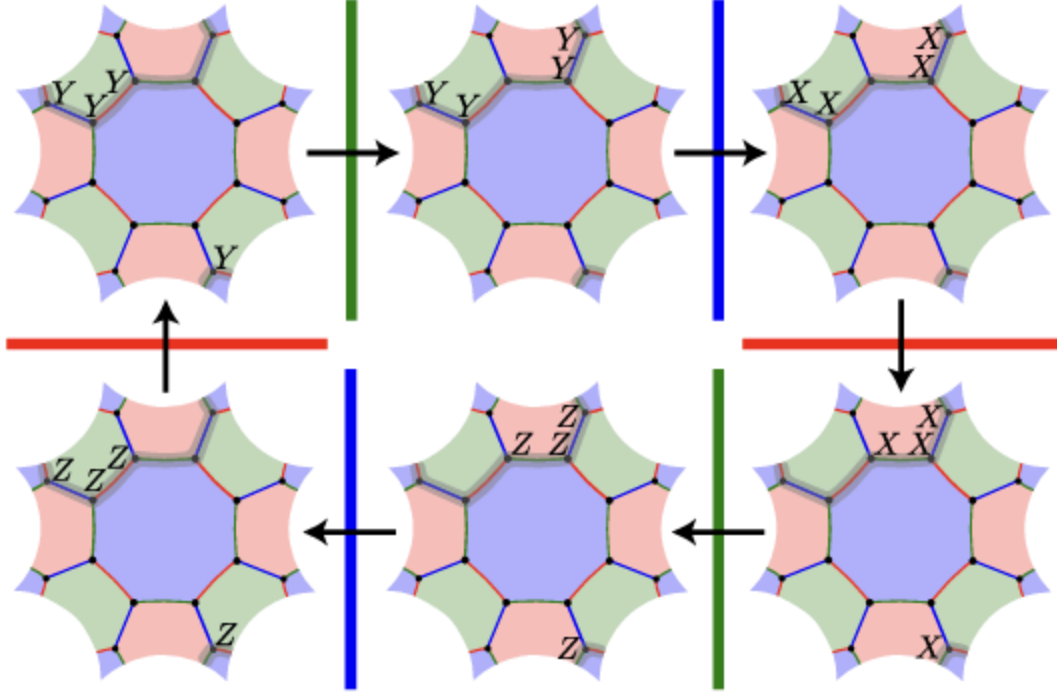
E. Circuits and noise models In this work we consider two different noise models, corresponding to the EM3 and SD6 noise models used in Ref. [22]. Both noise models are characterized by a noise strength parameter $p \in [0,1]$ (the physical error rate). 1. EM3 noise model The EM3 noise model (entangling measurement three step cycle) assumes that two-qubit Pauli measurements are available natively in the platform (and hence no ancilla qubits are needed), as is the case for Majorana-based architectures [20,29]. When implementing the measurement of a two-qubit Pauli operator $P_c \otimes P_c$, with probability p we insert an error chosen uniformly at random from the set $\{I, X, Y, Z\}^{\otimes 2} \times \{$flip,no flip$\}$. Here the two-qubit Pauli error in $\{I, X, Y, Z\}^{\otimes 2}$ is applied immediately before the measurement, and the "flip" operation flips the outcome of the measurement. We assume each measurement takes a single time step, and hence each cycle of three subrounds takes three time steps. Initialization of a qubit in the Z basis is followed by an X error, inserted with probability p/2. Similarly, the measurement of a data qubit in the Z basis is preceded by an X error, inserted with probability p/2. Single-qubit initialization and measurement in the X or Y basis is achieved using noisy Z-basis initialization or measurement and noiseless single-qubit Clifford gates. We do not need to define idling errors because data qubits are never idle in this noise model. 2. SD6 noise model The SD6 noise model (standard depolarizing six-step cycle) facilitates the check measurements via an ancilla qubit for each edge of the color-code tiling. Therefore, this noise model introduces $|E|=3|V|/2$ ancilla qubits and requires 2.5 times more qubits than the EM3 noise model for a given color-code tiling T. Note that the distance in this noise model (the minimum number of independent error mechanisms required to flip a logical observable but no detectors) can be higher than EM3 for a given tiling, so we do not necessarily require 2.5 times more qubits for a given distance.